Developmental Cell
Article

A Self-Organizing miR-132/Ctbp2 Circuit Regulates Bimodal Notch Signals and Glial Progenitor Fate Choice during Spinal Cord Maturation

Evgenia Salta,[1,2] Pierre Lau,[1,2] Carlo Sala Frigerio,[1,2] Marion Coolen,[3] Laure Bally-Cuif,[3] and Bart De Strooper[1,2,4,*]
[1]VIB Center for the Biology of Disease, 3000 Leuven, Belgium
[2]Center for Human Genetics and Leuven Institute for Neurodegenerative Disorders, KU Leuven, 3000 Leuven, Belgium
[3]Zebrafish Neurogenetics Group, Laboratory of Neurobiology and Development, CNRS UPR 3294, Institute of Neurobiology Alfred Fessard, Avenue de la Terrasse, 91198 Gif-sur-Yvette Cédex, France
[4]Institute of Neurology, University College London, Queen Square, WC1N 3BG London, UK
*Correspondence: bart.destrooper@cme.vib-kuleuven.be
http://dx.doi.org/10.1016/j.devcel.2014.07.006

SUMMARY

Radial glial progenitors play pivotal roles in the development and patterning of the spinal cord, and their fate is controlled by Notch signaling. How Notch is shaped to regulate their crucial transition from expansion toward differentiation remains, however, unknown. miR-132 in the developing zebrafish dampens Notch signaling via a cascade involving the transcriptional corepressor Ctbp2 and the Notch suppressor Sirt1. At early embryonic stages, high Ctbp2 levels sustain Notch signaling and radial glial expansion and concomitantly induce miR-132 expression via a double-negative feedback loop involving Rest inhibition. The changing balance in miR-132 and Ctbp2 interaction gradually drives the switch in Notch output and radial glial progenitor fate as part of the larger developmental program involved in the transition from embryonic to larval spinal cord.

INTRODUCTION

Radial glial progenitors play a critical role in the developing vertebrate central nervous system (CNS). They provide crucial scaffolding for neurite outgrowth and neuronal migration; they contribute to synaptic plasticity, they have self-renewal potential; and they also give rise to oligodendrocyte precursors, which, at later stages, myelinate axons (Campbell and Götz, 2002; Kim et al., 2008b). The radial glia and their processes actively contribute to the patterning of the developing spinal cord and to the conversion of the primitive lumen into the mature central canal (Barry et al., 2013; Givogri et al., 2006). This occurs during the transition from embryonic to fetal life in humans (between weeks 9 and 12 of intrauterine life) and from embryos to larvae during the hatching period in zebrafish (48–52 hr postfertilization [hpf]) (Kondrychyn et al., 2013; Sevc et al., 2009).

Notch signaling plays a key role in radial glial development (Taylor et al., 2007). Notably, the morphogenesis of the embryonic primitive lumen (up to around 48 hpf) is associated with increasing Notch signals and raising numbers of radial glial progenitors, whereas the transition to the central canal is paralleled by a gradual decrease of Notch signaling and a vast decline in progenitor cells that differentiate or become mitotically quiescent by 72 hpf (Hudish et al., 2013; Kim et al., 2008b).

Which epigenetic and posttranscriptional regulatory processes control Notch signaling dynamics in these cells remains, however, poorly understood (Kim et al., 2008a). Time-specific deletion of Dicer affects oligodendrocyte expansion and differentiation and impairs myelination (Kawase-Koga et al., 2009), but whether specific microRNAs (miRNAs) are involved and how these miRNAs could regulate Notch remain largely unknown.

We report here that miRNA-132 (miR-132) regulates Notch signaling in these progenitor cells. miR-132 is involved in dendritic and axonal growth and arborization, synaptic plasticity, and adult neurogenesis (Wanet et al., 2012), and it is significantly downregulated in several neurodegenerative and neurodevelopmental disorders (Jimenez-Mateos et al., 2011; Kim et al., 2010; Lau et al., 2013; Lee et al., 2011); however, its role in CNS development remains largely unknown. It is interesting that miR-132 is strongly expressed in Gfap^{+} glial progenitors in the developing zebrafish spinal cord. miR-132 loss of function resulted in dramatic alterations of the spinal cord morphology, inhibited the transition of radial glial progenitors to oligodendrocyte precursors, and eventually interfered with the normal development of the spinal central canal. We demonstrate that miR-132 is part of a bimodal regulatory network involving the transcriptional corepressor Ctbp2 and the Notch suppressor Sirt1.

RESULTS

miR-132 Is Required for Normal Glial Cell Development and Maturation of the Larval Spinal Cord

Expression of miR-132 is observed throughout the developing CNS (Figure 1A). The signal initially increases at 48 hpf and becomes 100-fold upregulated at 72 hpf (Figure 1B). In situ hybridization for miR-132 in larvae shows a pattern typical for radial glial progenitors (Figure 1A) (Kim et al., 2008b). miR-132 downregulation using a morpholino antisense oligonucleotide against the mature guide strand (miR-132 MO) persists until at least 72

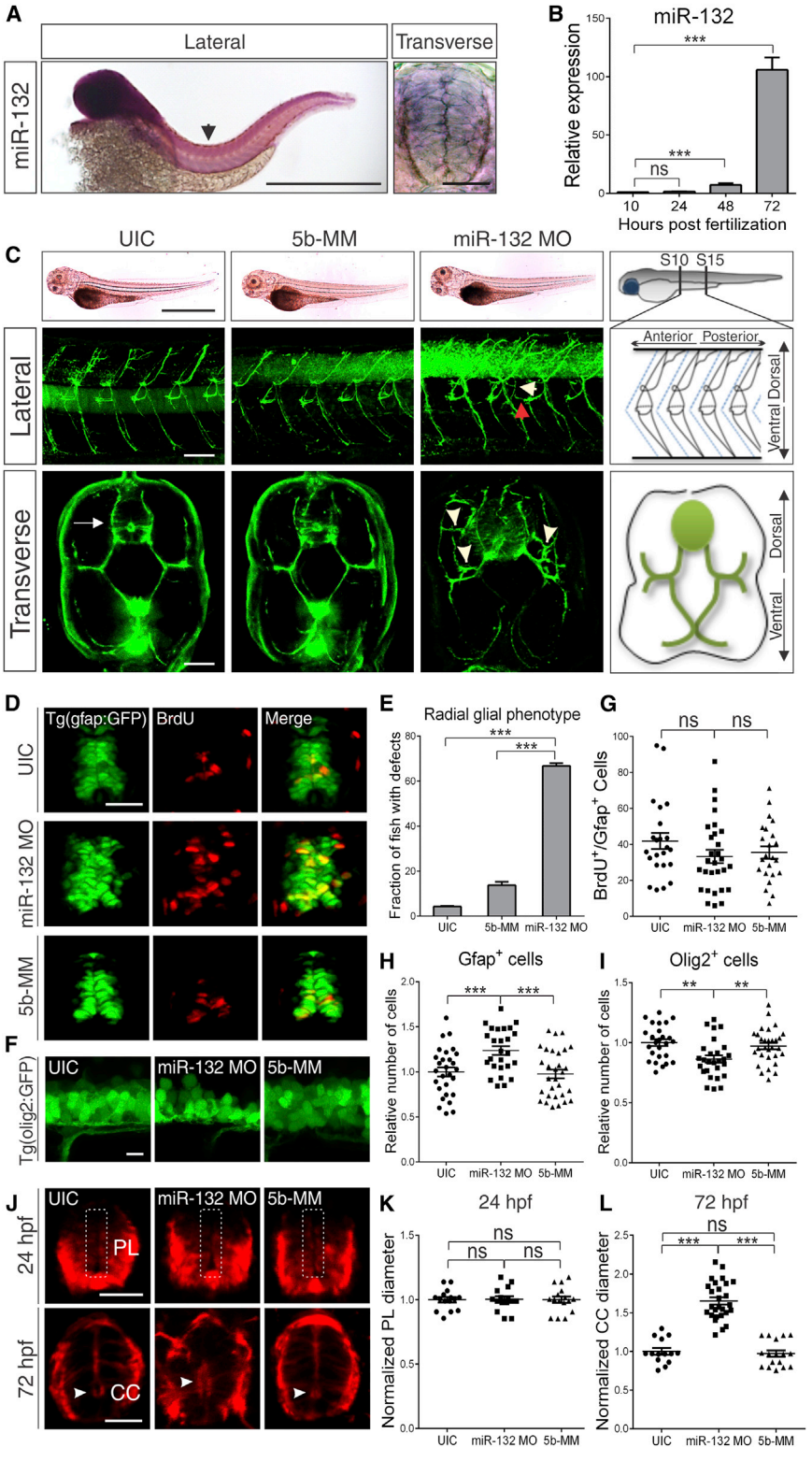

Figure 1. miR-132 Downregulation Causes Glial and Spinal Cord Maturation Deficits

(A) In situ hybridization of miR-132 at 48 hpf. Expression of miR-132 in the spinal cord (whole mount) and in the radial glial cells (cross-section). Arrowhead indicates region of cross-sectioning. Scale bars, 1 mm (lateral view); 4 μm (cross-section).

(B) Semiquantitative real-time PCR analysis of miR-132 expression in wild-type embryos and larvae at 10, 24, 48, and 72 hpf. Values were normalized to the U6 small nuclear RNA.

(C) miR-132 knockdown using an antisense morpholino. Top: Bright-field images of UIC, larvae injected with a 5b-MM or a morpholino against miR-132 (miR-132 MO) at 72 hpf, and schematic illustration of a zebrafish larva indicating the trunk region between S10 and S15 used to score the phenotypes. Scale bar, 1 mm. Middle: Lateral views of the trunk. The Gfap$^+$ glial processes are immunostained with zrf-1. White arrowhead indicates intraprocess ectopic branches. Red arrowhead indicates ectopic branch connecting two neighboring processes. Schematic illustration depicts a sagittal view of the perineural glial processes. Scale bar, 50 μm. Bottom: Cross-sections of the trunk immunostained with zrf-1. Arrow indicates the spinal cord. Arrowheads indicate ectopic branches. Schematic illustration depicts a transverse section showing the normal arborization pattern of glial processes. Scale bar, 10 μm.

(D) Transverse sections of the spinal cord of Tg(gfap:GFP) embryos after BrdU incorporation at 48 hpf, quantified in (G) and (H). Scale bar, 4 μm.

(E) Quantification of the Gfap$^+$ glial arborization defects in miR-132 morphants. Sample sizes: n = 172 for UIC; n = 132 for 5b-MM; and n = 195 for miR-132 MO.

(F) Lateral view of the spinal cord of miR-132 morphant and control Tg(olig2:GFP) embryos at 48 hpf, quantified in (I). Scale bar, 10 μm.

(G and H) Quantification of proliferating glial progenitors and of total number of progenitors. Values were expressed as percentage of BrdU-positive (BrdU$^+$) cells to total number of Gfap$^+$ cells within the spinal cord (G) or as total number of Gfap$^+$ cells (H).

(I) Quantification of the total number of oligodendrocyte lineage precursor cells at 48 hpf.

(J) Spinal cord cross-sections of miR-132 morphants (miR-132 MO) and controls immunostained with zrf-1 depicting the primitive lumen (dashed rectangle, PL) at 24 hpf or the central canal (arrowheads, CC) at 72 hpf. Scale bars, 4 μm.

(K and L) Quantification of the diameter of the primitive lumen (K) or the central canal (L) in miR-132 morphants and controls.

In (G) through (I), (K), and (L) each dot of the scatterplot represents the normalized average from four serial optical sections (z stacks) of one spinal cord cross-section per embryo. Values are presented as mean ± SEM. *p < 0.05; **p < 0.01; ***p < 0.001; ns, nonsignificant.

See also Figures S1 and S2.

hpf (Figure S1A available online). The miR-132 morphants display, at first glance, no gross morphological defects compared to uninjected controls (UIC) or embryos injected with a five base-mismatch control morpholino (5b-MM) (Figure 1C, top). However, miR-132 morphants exhibit impaired escape response to tactile stimulation on the trunk (Figure S1K). Immunostaining for pan-neuronal markers (anti-beta tubulin 1, Znp-1 [Zebrafish International Research Center; ZIRC] and Zna-1 [ZIRC]) does not depict any gross morphological abnormalities of neurons in brain and spinal cord, whereas anti-Gfap immunostaining reveals aberrant arborization of glial processes (Trevarrow et al., 1990) (Figure 1C, middle and bottom panel; Figure 1E). These Gfap$^+$ fibers are part of the perineurium, which originates from spinal cord radial glia. Its development is Notch dependent and plays an important role in the support and protection of motor neuron axons (Barresi et al., 2010; Kim et al., 2008a). We refer to them as "perineural glial processes." These perineural glial processes normally follow the somite segmentation pattern and project outside the spinal cord into the spinal myotome (Figure 1C, schematics). In the miR-132 morphants, branches develop ectopically and form connections across neighboring segments. A second morpholino directed against the precursor miR-132 (pre-miR-132) confirmed specificity (Figures S1B and S1C), while overexpressing miR-132 in the miR-132 morphants rescues the phenotype (Figure S1D).

Similar arborization phenotypes were observed in a mutagenesis screen affecting glial progenitors (Barresi et al., 2010). We therefore used transgenic markers to label radial glial cells [Tg(gfap:GFP)mi2001; Kim et al., 2008b] and (ventrally) located oligodendrocyte precursors [Tg(olig2:EGFP)vu12; Park et al., 2007; Shin et al., 2003]. The Olig2$^+$ precursors partially derive from Gfap$^+$ progenitors at early larval stages (Kim et al., 2008b) and give rise to neurons and oligodendrocytes (Barresi et al., 2010; Park et al., 2002; Petit et al., 2011; Zannino and Appel, 2009). Gfap immunostaining confirms that glial fibers from both the Gfap:green fluorescent protein (GFP)- and the Olig2:GFP-expressing populations (which display overlapping arborization profiles at this stage) are affected in miR-132 morphants (Figure S2). As Gfap:GFP$^+$ cells at postembryonic stages encompass bona fide radial glia but also some of their progeny, such as perineural glia, the Gfap:GFP$^+$ cells are collectively referred here to as Gfap$^+$ cells.

It is interesting that the number of Gfap$^+$ cells is elevated (Figures 1D and 1H), while the number of Olig2$^+$ cells is decreased (Figures 1F and 1I) in the miR-132 morphants. To assess their proliferation potential, we measured bromodeoxyuridine (BrdU) incorporation in the Gfap$^+$ progenitor cells (Figures 1D and 1G). The percentage of BrdU$^+$ cells to total number of Gfap$^+$ cells is not altered in the miR-132 morphants, indicating that their proliferative capacity is maintained. Opposite phenotypes—namely increased Olig2$^+$ population at the expense of the Gfap$^+$ pool—are seen when overexpressing miR-132 using a synthetic oligonucleotide (Figures S1E and S1F). We assessed the effect of miR-132 knockdown on the Olig2$^+$ cell progeny. We found that the proliferative capacity of the Sox10$^+$ oligodendrocyte precursors (Kim et al., 2008a) is compromised (Figure S3A), while the Isl1$^+$-primary motor neurons (Zannino and Appel, 2009) retain high levels of Gfap positivity (Figure S3B), indicating delayed or impaired motor neuron differentiation. Together, these observations show that miR-132 promotes the Olig2$^+$ progeny differentiation and proliferation over the Gfap$^+$ glial progenitor maintenance and expansion.

The gradual differentiation of the radial glial cells and the proper development of their arbors are involved in the transformation of the primitive spinal lumen into the mature central canal (Sevc et al., 2009). It is interesting that, while miR-132 deficiency does not cause any defects in the early lumen at 24 hpf (Figures 1J and 1K), miR-132 morphant spinal cords fail to complete the transition into the confined central canal at 72 hpf (Figures 1J and 1L).

We further investigated other possible downstream effects of the alterations in the cellular pool of progenitors. Olig2$^+$ precursors will further mature to myelinate axonal projections (Barresi et al., 2010). Myelin basic protein (Mbp) staining was decreased at 120 hpf (Figures S1G and S1I) (Buckley et al., 2010; Pogoda et al., 2006). Gfap$^+$ glia also act as a scaffold for the neuritic pathfinding of motor neurons (Barresi et al., 2010). Immunostaining against acetylated tubulin (AcTub) confirms that most of the ectopic Gfap$^+$ glial projections are accompanied by newly formed misrouted AcTub$^+$ neurites (Figures S1H and S1J). In conclusion, the miR-132 loss-of-function phenotype is characterized by a perturbed balance of Gfap$^+$ and Olig2$^+$ glial cells and aberrant perineural glial process formation. This correlates with impaired differentiation of the Olig2$^+$ progeny, disorganized neurite outgrowth, delayed myelination, and abnormal spinal central canal formation.

Notch Signaling Mediates the miR-132 Effects

Activation of Notch signaling is associated with delayed neurogenesis, increased gliogenesis, impaired maturation of oligodendrocytes, and myelination (Taylor et al., 2007; Wang et al., 1998). To monitor Notch signaling in miR-132 morphants, we assessed the expression of *her4*, a gene encoding a basic helix-loop-helix Enhancer-of-split transcription factor (Takke et al., 1999; Yeo et al., 2007). It is important to note that, although *her4* is not a predicted miR-132 target, downregulation of miR-132 leads to its upregulation (Figure 2A), while overexpressing miR-132 represses its expression (Figure 2B). To rule out that the observed effects on *her4* might simply reflect changes in progenitor cell numbers rather than variations in cellular *her4* transcription, we used fluorescence-activated cell sorting (FACS) to sort GFP$^+$ glial cells from Tg(gfap:GFP) miR-132 morphant embryos. Elevated *her4* levels per cell were confirmed in these samples (Figure 2C).

We confirmed the role of Notch signaling in the miR-132 morphant phenotype using the well characterized γ-secretase inhibitor N-[N-(3,5-difluorophenacetyl)-L-alanyl]-S-phenylglycine t-butyl ester (DAPT) (Geling et al., 2002) to inhibit Notch from 24 hpf on, thus covering the period when the Notch pathway has been shown to actively instruct the radial glial cell fate and arborization (Kim et al., 2008b). DAPT represses *her4* transcription in the zebrafish spinal cord (Kim et al., 2008b). In a titration assay (Figure S3C), we found that a concentration of 5 μg/ml indeed reverses *her4* upregulation in miR-132 morphants (Figure 2D) and normalizes Gfap$^+$ and Olig2$^+$ cell numbers back to control levels (Figures 2E and 2F). Notably, the same concentration of DAPT in wild-type embryos leads to an inverse shift in *her4* expression levels and the glial progenitor

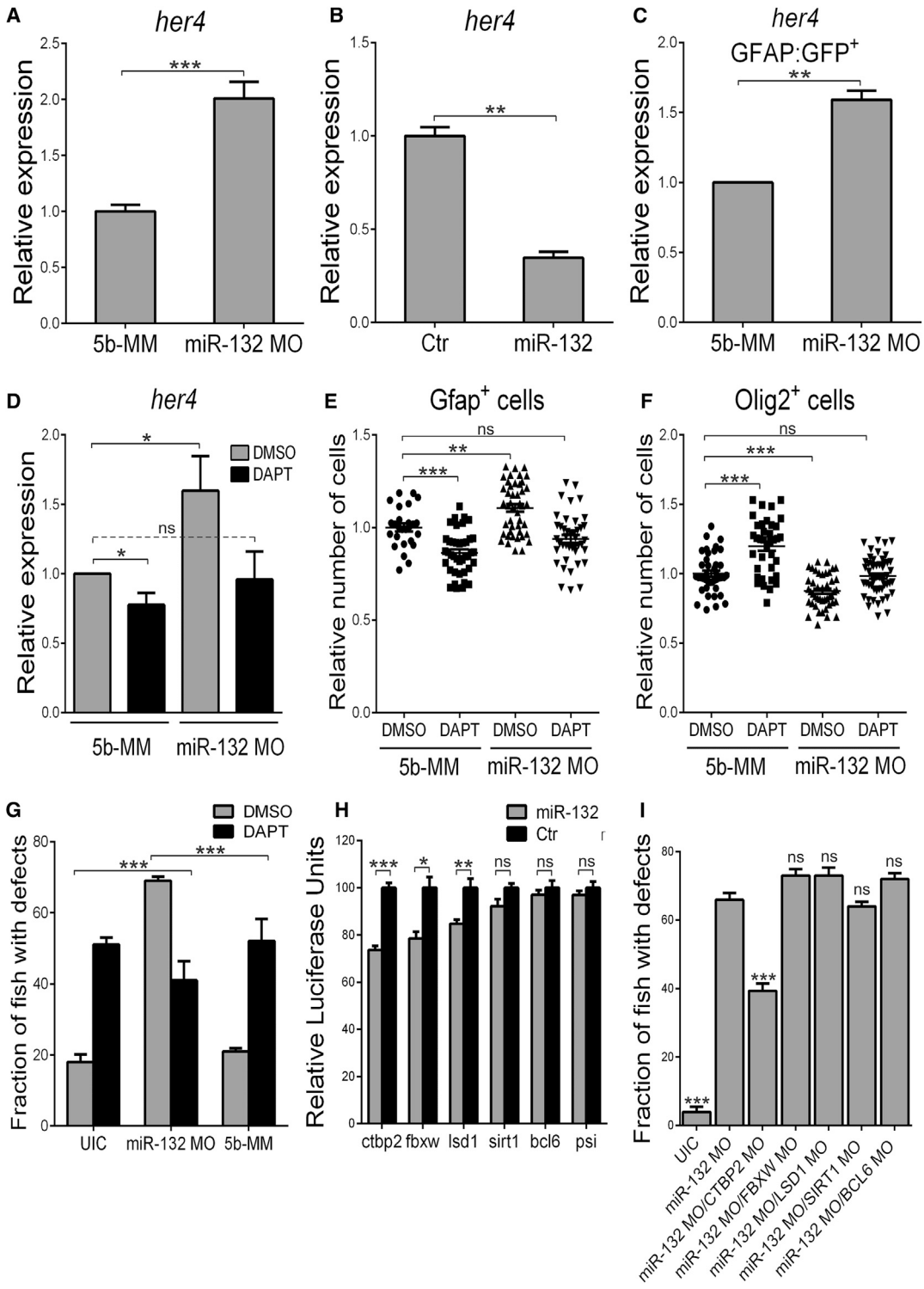

Figure 2. miR-132 Regulates Glial Progenitors through Notch

(A and B) Semiquantitative real-time PCR analysis showing *her4* expression in miR-132 morphant embryos (miR-132 MO) compared to embryos injected with control morpholino (5b-MM) (A) or in embryos injected with a miR-132 mimic (miR-132) compared to embryos injected with a control oligonucleotide (Ctr), at 10 hpf (B).

(C) Semiquantitative real-time PCR analysis showing upregulation of *her4* expression in gfap:GFP$^+$ FACS-sorted cells isolated from Tg(gfap:GFP) miR-132 morphants compared to control larvae, at 24 hpf.

(D) *her4* expression in miR-132 morphant and control larvae at 48 hpf following 24 hr incubation in DAPT or vehicle control (DMSO).

(legend continued on next page)

balance (Figures 2D–2F); thus, the Notch signal dose is critical in both directions for proper glial cell development. Finally, DAPT incubation partially rescues the glial arborization phenotype in the miR-132 morphants (Figure 2G). Together, these series of data demonstrate a critical role for miR-132 in fine tuning of the Notch signal in this context.

We used a candidate gene approach to identify miR-132 targets. Using computational algorithms (see Experimental Procedures), we identified five putative miR-132 targets in the Notch pathway that were conserved across *Danio rerio*, *Homo sapiens*, and/or *Mus musculus*: C-terminal binding protein (*ctbp2*) (NM_131715.1); F box and WD-40 domain protein 11b (*fbxw11b*) (NM_213504.2); lysine (K)-specific demethylase 5Ba (*kdm5ba* or *lsd1*) (NM_001128327.1); silent mating type information regulation 2 homolog 1 (*sirt1*) (XM_001334404.4); and Bcl6 corepressor (*bcor*) (NM_205626.1). To assess the functional relevance of these candidates, we cloned their 3′ untranslated region (UTR) downstream of the renilla *luciferase* gene and cotransfected human embryonic kidney 293 (HEK293) cells along with a miR-132 mimic oligonucleotide. The most significant reduction of luminescence is observed for the 3′ UTR of *ctbp2*, while more modest downregulation is observed for *fbxw11b* and *lsd1* (Figure 2H). We then asked which of these five candidate genes could be involved in the miR-132 morphant glial arborization phenotype in vivo (Figure 2I). Notably, only knocking down Ctbp2 can rescue the branching defects in the miR-132 morphants.

miR-132 Directly Targets the Transcriptional Corepressor Ctbp2

We next performed loss-of-function, epistasis, and gain-of-function experiments to demonstrate that the transcriptional corepressor Ctbp2 is necessary and sufficient for mediating the miR-132 effects on the radial glial cell population.

Lowering Ctbp2 levels in wild-type fish using a morpholino against Ctbp2 is sufficient to downregulate *her4* expression (Figure 3A) and shifts the glial progenitor population toward the Olig2$^+$ lineage (Figures 3B and 3C), opposite to the effects observed on miR-132 downregulation. Conversely, a similar Ctbp2 loss of function in miR-132 morphants causes normalization of *her4* levels (Figure 3A) and restores the Gfap$^+$/Olig2$^+$ balance (Figures 3B and 3C). The knockdown efficiency of Ctbp2 is approximately 50%, as confirmed by western blot (Figure S4A). This epistasis experiment demonstrates the critical role of Ctbp2 and miR-132 in the regulation of the Notch signal in the Gfap$^+$/Olig2$^+$ cells.

To confirm that upregulation of Ctbp2 in the Gfap$^+$ glial progenitors is indeed sufficient to explain the glial arborization phenotype, we injected embryos with a construct containing the *ctbp2* gene under the regulatory promoter elements of *gfap*, thus driving Ctbp2 expression primarily in the radial glial cellular population (Figure 3D). The specificity of the *gfap* promoter construct was tested using mCherry. It is interesting that overexpression of Ctbp2 in the radial glial progenitors alone mimics the glial arborization abnormalities observed on miR-132 knockdown (Figure 3F). We then confirmed that lowering Ctbp2 expression in the miR-132 morphants rescues the miR-132 arborization phenotype (Figure 2I) using a second morpholino (Figures 3E and 3G). This rules out off-target effects as the two morpholinos inhibit the expression of Ctbp2 via different mechanisms, i.e., through blocking the translational initiation or through hindering messenger RNA (mRNA) splicing. We finally confirmed that Ctbp2 protein levels are significantly increased in the miR-132 morphants (Figure 3H), further establishing the functional link between miR-132 and Ctbp2 in vivo.

While our experiments strongly suggest that Ctbp2 is the main target of miR-132 in the described phenotypes, it is still possible that other miR-132 targets may contribute to the effects. We therefore used target protector morpholinos (Staton and Giraldez, 2011) against two putative miR-132 miRNA response elements (MREs) in the *ctbp2* 3′ UTR (Figure 4A). A third morpholino targeting a truncated binding site was used as a negative control. Blocking the miR-132 MREs on the *ctbp2* 3′ UTR with each one of the first two target protectors is indeed sufficient to increase *her4* levels (Figure 4B) and to induce the shift of the glial progenitor pool toward the Gfap$^+$ cell lineage (Figures 4C and 4D). Moreover, the injected larvae display glial arborization defects that are similar to the miR-132 morphants (Figures 4E and 4F). Codownregulation of Ctbp2 largely rescues the arborization phenotype (Figures 4E and 4F), indicating that the target protectors specifically block the interaction between miR-132 and *ctbp2* transcript.

This series of data unequivocally demonstrates that the endogenously expressed Ctbp2 represents the direct and major in vivo target of endogenous miR-132 in the context of the radial glial progenitors at this developmental stage and that abrogation of this interaction is sufficient to explain the effects of miR-132 loss of function on glial development.

The Histone Deacetylase Sirt1 Acts Downstream of Ctbp2

It remains unclear how Ctbp2, which is a transcriptional corepressor, can positively affect Notch. The histone deacetylase Sirt1 is known to suppress Notch signaling and is repressed by

(E and F) Effect of DAPT incubation of miR-132 morphant and control larvae on the total number of Gfap$^+$ (E) and Olig2$^+$ (F) cells in the spinal cord of Tg(gfap:GFP) (E) or Tg(olig2:GFP) (F) larvae at 48 hpf. Each dot of the scatterplot represents the normalized average from four serial optical sections (z stacks) of one spinal cord cross-section per embryo.

(G) Quantification of the glial arborization phenotype at 72 hpf in UIC, miR-132 MO, and 5b-MM larvae following 48 hr incubation in DAPT or vehicle control (DMSO). Sample sizes: n = 114 for UIC-DAPT; n = 97 for UIC-DMSO; n = 81 for miR-132 MO-DAPT; n = 72 for miR-132 MO-DMSO; n = 71 for 5b-MM-DAPT; and n = 67 for 5b-MM-DMSO.

(H) Luciferase assay of candidate target 3′ UTRs. Cells were cotransfected with a miR-132 mimic (miR-132) or a control oligonucleotide (Ctr). Values were normalized against firefly luciferase expression and expressed as percentage compared to the control.

(I) Effect of codownregulating miR-132 and the candidate targets on the glial arborization phenotype at 72 hpf. Values were compared to miR-132 morphant group. Sample sizes: n = 58 for UIC; n = 50 for miR-132 MO; n = 91 for miR-132 MO/CTBP2 MO (translation blocking MO); n = 88 for miR-132 MO/FBXW MO; n = 96 for miR-132 MO/LSD1 MO; n = 92 for miR-132 MO/SIRT1 MO; and n = 96 for miR-132 MO/BCL6 MO.

In (A) through (D), values were normalized to the geometric mean of *ef1a*, *b2m*, and *actin* and expressed as fold change compared to the control. Values are presented as mean ± SEM. *p < 0.05; **p < 0.01; ***p < 0.001; ns, nonsignificant. See also Figure S3.

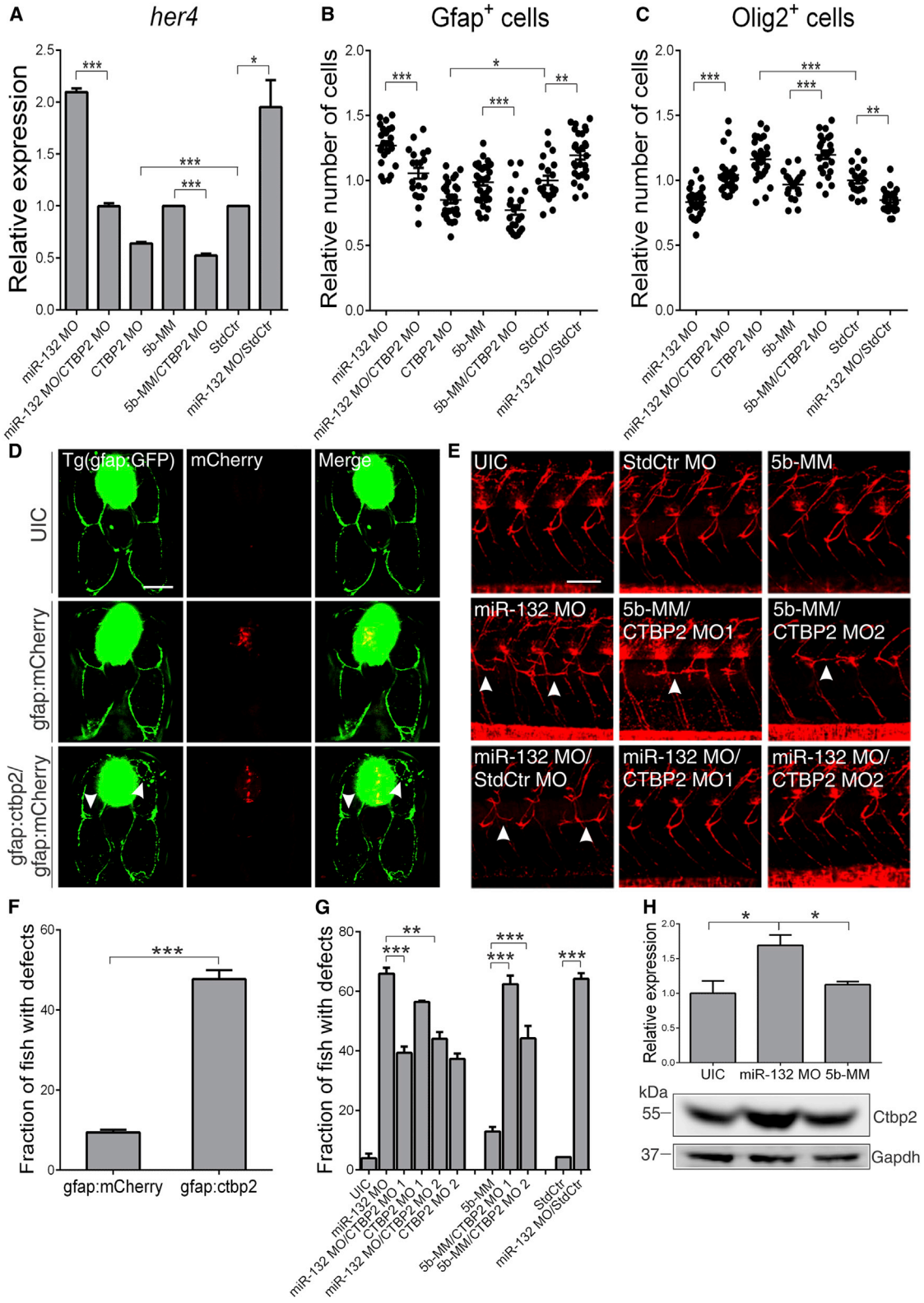

Figure 3. The miR-132 Morphant Phenotype Is Mediated through the Transcriptional Corepressor Ctbp2

(A) Semiquantitative real-time PCR analysis showing the effect of Ctbp2 downregulation on *her4* levels (CTBP2 MO, splice blocking morpholino) in miR-132 morphant and control embryos at 24 hpf. Values were normalized to the geometric mean of *ef1a*, *b2m*, and *actin* and expressed as fold change compared to the control.

(legend continued on next page)

Ctbp2 (Guarani et al., 2011; Mulligan et al., 2011; Zhang et al., 2007). We therefore hypothesized that Sirt1 might be one of the downstream targets of Ctbp2 in this pathway (Figure 5A). Indeed, Sirt1 deficiency causes upregulation of *her4* (Figure 5B), a shift toward the Gfap$^+$ progenitor state (Figures 5C and 5D), and glial arborization abnormalities (Figures 5E and 5F). The efficiency of the Sirt1 knockdown was about 60% (Figure S4B). The specificity of the morpholino effect was demonstrated by rescuing the Sirt1 morphant phenotype via glia-specific overexpression of Sirt1 (injecting embryos with a construct expressing Sirt1 under the regulatory elements of *gfap*) (Figure S4C). More important, epistasis experiments show that Sirt1 is involved in the miR-132 morphant phenotype: radial glia-specific overexpression of Sirt1 rescues the miR-132 loss-of-function arborization phenotype (Figures 5G and 5H). Biochemical analysis further corroborates that miR-132 knockdown results in a decrease of *sirt1* transcript levels (Figure 5I). We then assessed the regulatory effect of Ctbp2 over Sirt1. The levels of *sirt1* are elevated in the Gfap:GFP$^+$ fraction of the Ctbp2 morphants (Figure 5J), while Sirt1 knockdown in Ctbp2 morphants significantly rescues the glial arborization phenotype (Figure 5K). Notably, and confirming the link to the Notch pathway, treatment with 5 μg/ml DAPT rescues the Sirt1 morphant phenotype (Figure 5L).

Ctbp2 Induces Its Own Suppressor

miR-132 levels are not very high in the early embryonic stages but become dramatically upregulated from 48 hpf on (Figure 1B). While the mRNA of Ctbp2 exhibits a similar profile, Ctbp2 protein is strongly downregulated after 48 hpf (Figures 6A and 6B). miR-132 plays a crucial role in this downregulation as demonstrated earlier. However, the coherent coexpression pattern of Ctbp2 and miR-132 until 48 hpf raised the question of whether Ctbp2 itself could build up miR-132 expression during embryonic stages (Peng et al., 2012).

In such a scenario, shifting Ctbp2 upregulation to earlier embryonic stages should correspondingly shift miR-132 induction. Indeed, radial glia-specific overexpression of Ctbp2 increases miR-132 levels already at 24 hpf (Figure 6C). Moreover, Ctbp2 knockdown led to miR-132 downregulation at 48 hpf (Figure 6C). Thus, Ctbp2 appears able to regulate its own suppressor within the time window ranging from early embryonic (24 hpf) to late embryonic/early larval (48 hpf) life. Since Ctbp2 is a transcriptional repressor, the effect should be mediated by an additional suppressor. Rest is a miR-132 repressor and a reported transcriptional target of Ctbp2 (Conaco et al., 2006; Johnson and Buckley, 2009; Liang et al., 2011; Wu and Xie, 2006). Rest expression is high early in embryogenesis and gradually declines until 72 hpf (Figure S5A). Downregulating Rest led to a significant upregulation of miR-132 at 48 hpf (Figure 6D). This upregulation is sufficient to prematurely downregulate *ctbp2* already at this time point (Figure 6D). The double negative feedback loop between Ctbp2, Rest, and miR-132 was finally corroborated with an epistasis experiment, in which the effect of Ctbp2 downregulation on miR-132 expression was rescued in Rest morphants (Figure 6E). We also confirm that changes in Rest expression affected the *her4* increase (Figure 6F) and the Gfap$^+$ glial number elevation (Figure 6G) from 24 hpf to 48 hpf, in agreement with a derepression of miR-132 and an out-of-phase downregulation of Ctbp2. Thus, in the absence of Rest, the transition to the late larval state is accelerated. Of note, *sirt1* endogenous expression profile is inversely correlated to the one of Ctbp2, in agreement with the physiological significance of the described regulatory circuitry (Figure S5B). We further verified the expression of *ctbp2* and *sirt1* in the Gfap$^+$ glial progenitors, confirming that, along with miR-132, the other components of the described signaling pathway are also expressed in these cells (Figure S6).

Our data imply that Ctbp2 interacts with miR-132 in different modes in embryonic and larval stages: in the embryo, with high Ctbp2 and low miR-132 levels, Ctbp2 predominantly induces miR-132; in the larva, miR-132, at high levels, buffers Ctpb2 expression. In this case, the decreased expression of miR-132 observed in Ctbp2 morphants should reflect an early effect of Ctbp2 over miR-132. To confirm this, we used a photomorpholino (Tallafuss et al., 2012) against Ctbp2 (Figure 6H) to specifically downregulate Ctbp2 at 34 hpf or 56 hpf. Notably, exposure to UV light did not induce any changes on Ctbp2 and miR-132 levels in UIC controls (Figure S5C), while the photomorpholino did not affect Ctbp2 protein levels in the injected but non-UV-illuminated group (Figure S5D). Although UV treatment of photomorpholino-injected embryos at 34 hpf and larvae at 56 hpf resulted in a similar Ctbp2 downregulation (Figure 6I), miR-132 was downregulated on UV illumination at 34 hpf but not at 56 hpf (Figure 6I).

Taken together, our data support a developmentally controlled bimodal regulatory circuit between miR-132 and Ctbp2, which shapes the Notch signal output and the glial progenitor density in the developing spinal cord (Figure 7).

(B and C) Effect of Ctbp2 downregulation using a splice blocking morpholino on the total number of Gfap$^+$ (B) and Olig2$^+$ (C) in the spinal cord of Ctbp2 morphant and control Tg(gfap:GFP) (B) or Tg(olig2:GFP) (C) embryos at 48 hpf. Each dot of the scatterplot represents the normalized average from four serial optical sections (z stacks) of one spinal cord cross-section per embryo.

(D) Transverse trunk sections of Tg(gfap:GFP) larvae either UIC, overexpressing gfap:mCherry (mCherry under the *gfap* promoter), or gfap:ctbp2 (*ctbp2* under the *gfap* promoter) in a mixture with gfap:mCherry at 72 hpf. Quantified in (F). Scale bar, 10 μm. Arrowheads indicate aberrant arborization of glial processes.

(E) Zrf-1 immunostaining of whole mounts at 72 hpf, lateral views of trunk. StdCtr MO, standard control morpholino; CTBP2 MO1, translation blocking morpholino against Ctbp2; CTBP2 MO2, splice blocking morpholino against Ctbp2. Quantified in (G). Scale bar, 50 μm. Arrowheads indicate aberrant arborization of glial processes.

(F) Quantification of glial arborization phenotype at 72 hpf in gfap:Ctbp2-overexpressing larvae and control larvae overexpressing gfap:mCherry. Sample size, n = 75 for gfap:Ctbp2; n = 71 for gfap:mCherry.

(G) Quantification of glial arborization phenotype in miR132/Ctbp2 double morphants at 72 hpf. Sample sizes: n = 162 for UIC; n = 186 for miR-132 MO; n = 128 for CTBP2 MO1; n = 86 for miR-132 MO-CTBP2 MO1; n = 118 for CTBP2 MO2; n = 100 for miR-132 MO/CTBP2 MO2; n = 125 for 5b-MM; n = 70 for 5b-MM/CTBP2 MO1; n = 61 for 5b-MM/CTBP2 MO2; n = 120 for StdCtr; and n = 103 for miR-132 MO/StdCtr.

(H) Western blot analysis of Ctbp2 protein levels in miR-132 morphants compared to control groups at 72 hpf. Protein levels were normalized against Gapdh. Values are presented as mean ± SEM. *$p < 0.05$; **$p < 0.01$; ***$p < 0.001$; ns, nonsignificant. See also Figure S4.

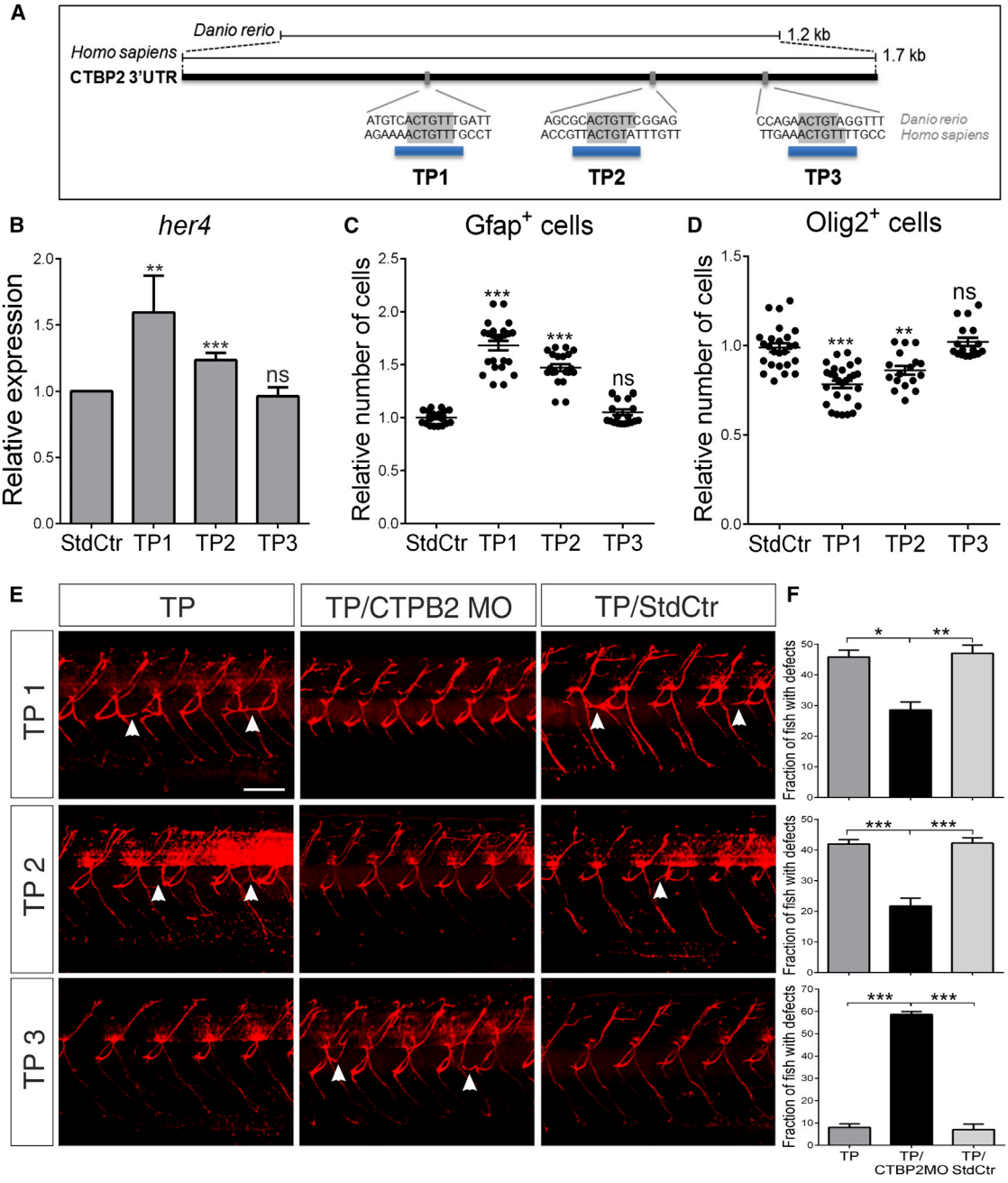

Figure 4. miR-132 Regulates Ctbp2 Levels by Directly Binding to Its 3′ UTR

(A) Schematic illustration of the miR-132 MREs in the 3′ UTR of *Ctbp2* in zebrafish (*Danio rerio*) and human (*Homo sapiens*) showing the three sites selected for the targeting by target protector morpholinos (TPs).

(B) Semiquantitative PCR analysis of the effect of the TPs on *her4* expression at 72 hpf. Values were normalized to the geometric mean of *ef1a*, *b2m*, and *actin* and expressed as fold change compared to the control.

(C and D) Effect of the TPs on the total number of Gfap$^+$ (C) and Olig2$^+$ (D) in the spinal cord of morphant and control Tg(gfap:GFP) (C) or Tg(olig2:GFP) (D) embryos at 48 hpf. Each dot of the scatterplot represents the normalized average from four serial optical sections (z stacks) of one spinal cord cross-section per embryo. Values were compared to the control-injected group.

(E) Zrf-1 immunostaining of whole mounts at 72 hpf, lateral views of trunk. Arrowheads indicate ectopic branches of Gfap$^+$ glial processes. TP, target protector morphants; TP/CTBP2 MO, target protector morphants coinjected with a translation blocking morpholino against Ctbp2; TP/Std Ctr, target protector morphants coinjected with a standard control morpholino. Scale bar, 50 μm.

(F) Quantification of glial arborization phenotype at 72 hpf. Sample sizes: n = 132 for TP1; n = 90 for TP1/CTBP2 MO; n = 104 for TP1/Std Ctr; n = 142 for TP2; n = 116 for TP2/CTBP2 MO; n = 107 for TP2/Std Ctr; n = 128 for TP3; n = 80 for TP3/CTBP2 MO; and n = 72 for TP3/Std Ctr.

Values are presented as mean ± SEM. *p < 0.05; **p < 0.01; ***p < 0.001; ns, nonsignificant.

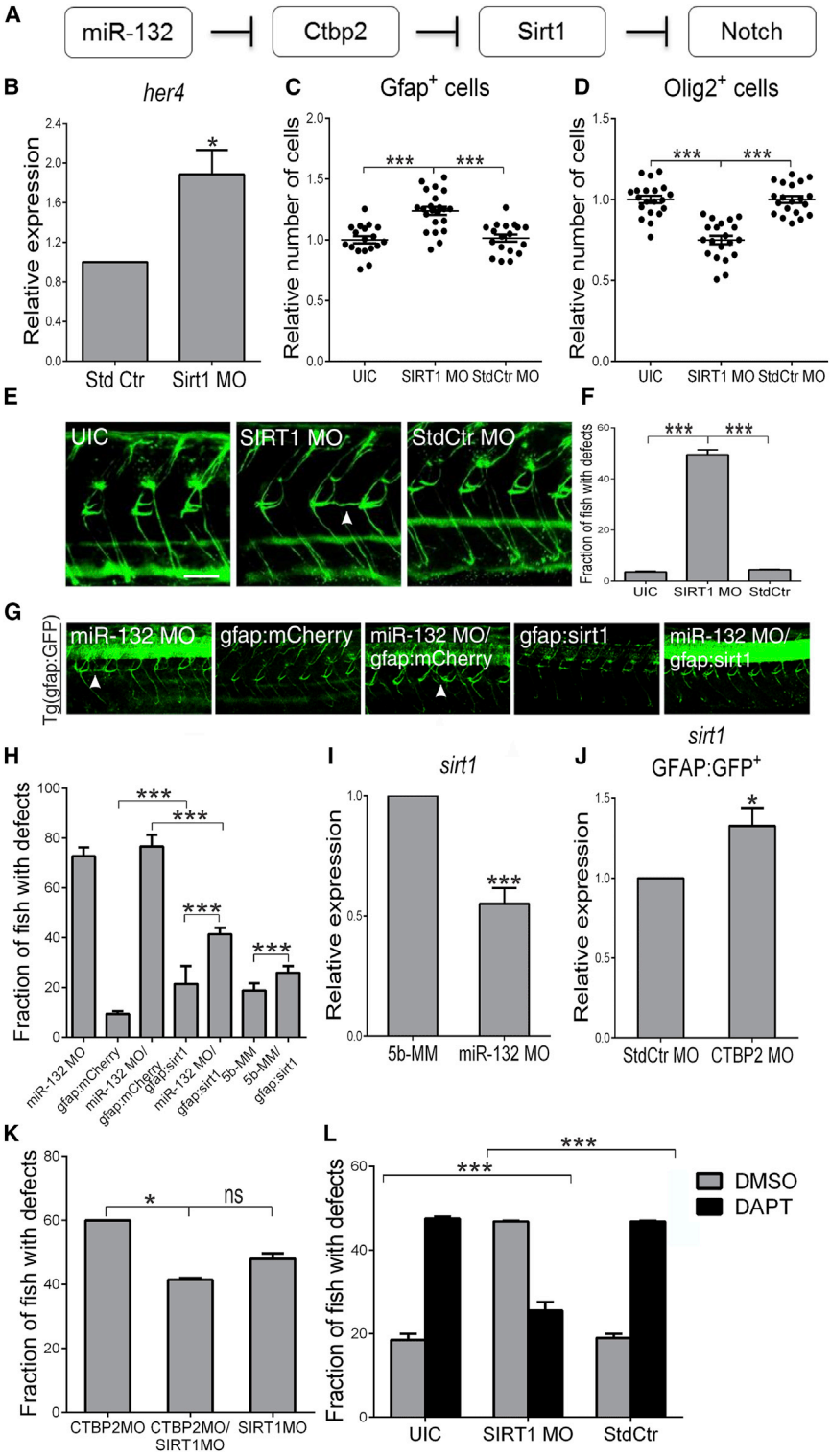

Figure 5. The Histone Deacetylase Sirt1 Is Regulated by miR-132 and Ctbp2

(A) Model of Sirt1 involvement in the miR-132/Ctbp2/Notch regulatory pathway.

(B) Semiquantitative PCR analysis of *her4* expression levels in Sirt1 morphants (SIRT1 MO) and control embryos (Std Ctr) at 24 hpf. Values were normalized as described earlier.

(C and D) Effect of Sirt1 downregulation (SIRT1 MO) on the total number of Gfap$^+$ (C) and Olig2$^+$ (D) in the spinal cord of Sirt1 morphant and control Tg(gfap:GFP) (C) or Tg(olig2:GFP) (D) embryos at 48 hpf. Each dot of the scatterplot represents normalized averages as described earlier.

(E) Whole-mount immunostaining with zrf-1 at 72 hpf, lateral views of trunk. SIRT1 MO, Sirt1 morphants; StdCtr MO, larvae injected with standard control morpholino. Scale bar, 50 μm.

(F) Quantification of glial arborization phenotype in Sirt1 morphants at 72 hpf. Sample size, n = 75 for UIC; n = 90 for SIRT1 MO; n = 95 for StdCtr MO.

(G) Lateral trunk views of 72 hpf – larvae injected with miR-132 morpholino (miR-132 MO), gfap:mCherry (*mCherry* under the *gfap* promoter), gfap:sirt1 (*sirt1* under the *gfap* promoter) or coinjected with miR132 morpholino and gfap:mCHERRY or miR-132 morpholino and gfap:sirt1. Scale bar, 50 μm. In (E) and (G), arrowheads indicate ectopic Gfap$^+$ glial processes.

(H) Quantification of the partial rescue of the glial arborization phenotype in the miR-132 morphants overexpressing Sirt1 under the *gfap* promoter at 72 hpf. Sample sizes: n = 52 for miR-132 MO; n = 61 for gfap:mCherry; n = 57 for miR-132 MO/gfap:mCherry; n = 63 for gfap:sirt1; n = 72 for miR-132 MO/gfap:sirt1; n = 70 for 5b-MM; and n = 58 for 5b-MM/gfap:sirt1.

(I and J) Semiquantitative real-time PCR analysis showing expression of *sirt1* in miR-132 morphant (miR-132 MO) and control embryos (5b-MM) at 24 hpf (I) or in gfap:GFP$^+$ FACS-sorted cells isolated from Tg(gfap:GFP) Ctbp2 morphants compared to control larvae, at 72 hpf (J). Values were normalized as described earlier.

(K) Quantification of glial arborization phenotype in Ctbp2/Sirt1 double morphants. Sample sizes: n = 78 for CTBP2 MO (translation blocking morpholino); n = 95 for CTBP2 MO/SIRT1 MO; and n = 87 for SIRT1 MO.

(L) Quantification of the glial arborization phenotype at 72 hpf in UIC, Sirt1 morphants (SIRT1 MO), and larvae injected with a standard control morpholino (StdCtr) following 48 hr incubation in DAPT or vehicle control (DMSO). Sample sizes: n = 87 for UIC-DAPT; n = 74 for UIC-DMSO; n = 66 for SIRT1 MO-DAPT; n = 69 for SIRT1 MO-DMSO; n = 54 for StdCtr-DAPT; and n = 66 for StdCtr-DMSO. Values are presented as mean ± SEM. *$p < 0.05$; ***$p < 0.001$; ns, nonsignificant.

DISCUSSION

We identify a temporally controlled bidirectional regulatory circuit between miR-132 and its target Ctbp2, which ultimately shapes the dynamics of Notch signaling and its output in the glial progenitors. During early embryonic development, Ctbp2 is gradually increasing, thereby inducing Notch signaling via Sirt1 transcriptional repression. This leads to progressive expansion of the Gfap$^+$ glial progenitor pool from 24 to 48 hpf. Ctbp2 also induces miR-132 expression through a double negative

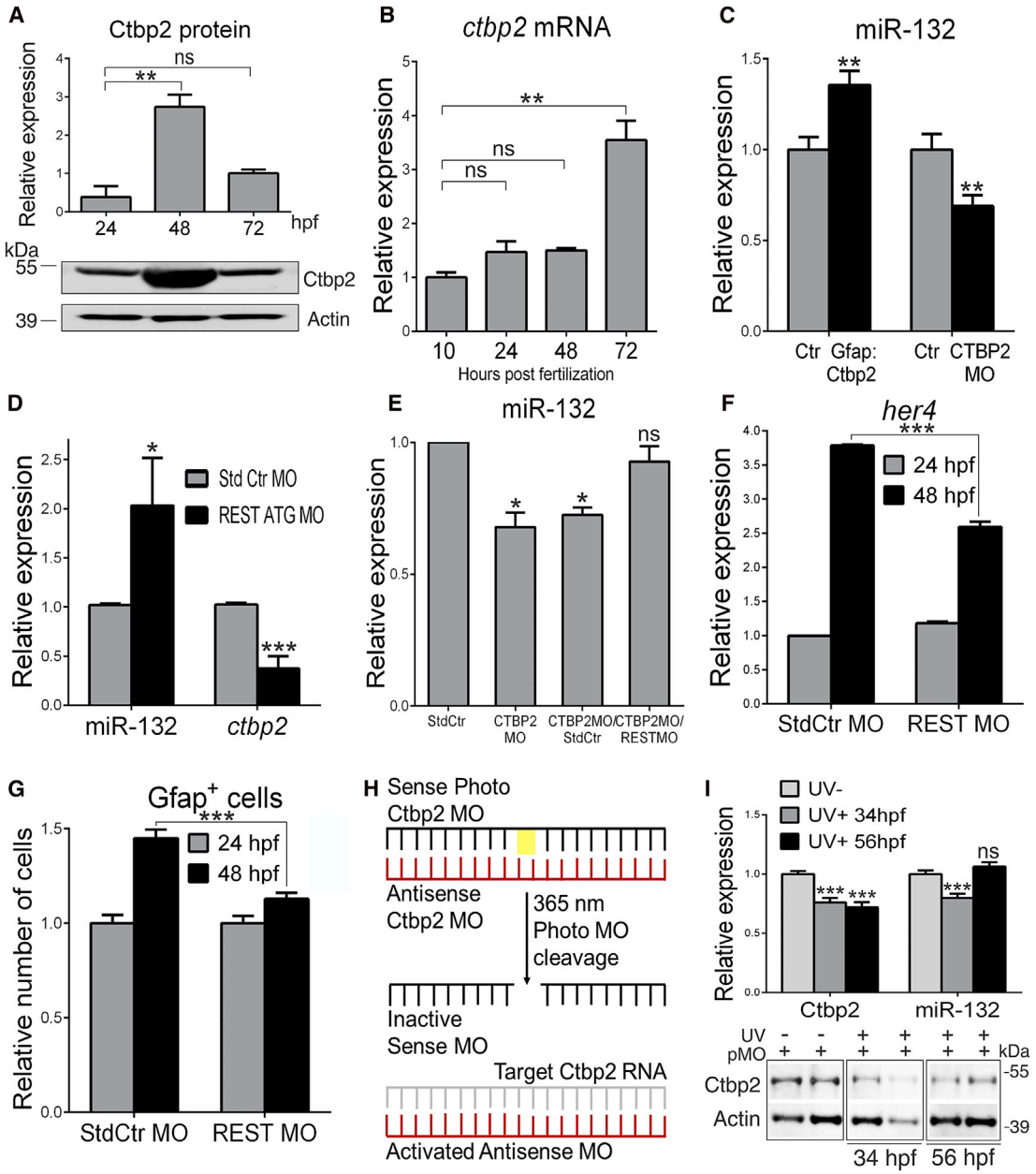

Figure 6. Feedback Regulation of miR-132 by Ctbp2 Is Controlled in a Time-Specific Manner

(A) Western blot analysis of Ctbp2 protein levels in wild-type embryos and larvae at 24, 48, and 72 hpf. Protein levels were normalized against Actin.

(B) Semiquantitative real-time PCR analysis of *ctbp2* expression in wild-type embryos and larvae at 10, 24, 48, and 72 hpf.

(C) miR-132 expression upon overexpression of Ctbp2 in radial glial progenitor cells (*ctbp2* under the *gfap* promoter) at 24 hpf and following downregulation of Ctbp2 with a splice blocking morpholino (CTBP2 MO) at 48 hpf. Values were normalized to the control gfap:mCherry-injected group (*mCherry* under the *gfap* promoter) or to the control-injected group (StdCtr MO), respectively.

(D) Semiquantitative real-time PCR analysis of miR-132 and *ctbp2* transcripts on downregulation of Rest at 48 hpf using a translation blocking morpholino (REST ATG MO).

(E) Semiquantitative real-time PCR analysis of miR-132 levels in Ctbp2 (splice blocking morpholino)-Rest double morphants (CTBP2 MO/REST MO) at 48 hpf. Values were normalized to the control-injected group (StdCtr).

(F) Semiquantitative PCR analysis of *her4* expression levels in Rest morphants (REST MO) and controls (StdCtr MO) during the transition from 24 to 48 hpf. Values were normalized to *her4* levels at 24 hpf.

(G) Quantification of the number of Gfap$^+$ cells in the spinal cord of Rest morphants and controls during the transition from 24 to 48 hpf. Values were normalized to the number of the cells at 24 hpf.

(H) Schematic illustration of the photomorpholino mechanism used for the time-specific downregulation of Ctbp2.

(legend continued on next page)

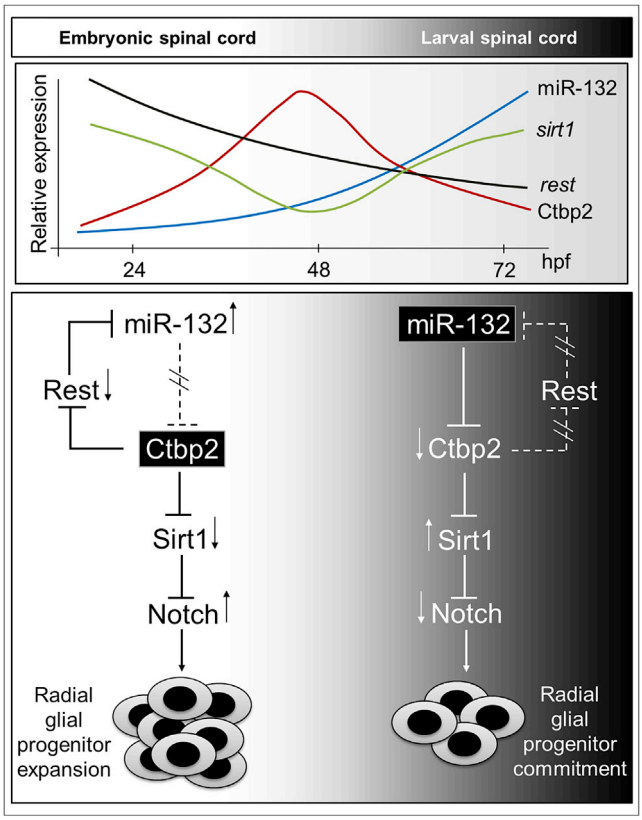

Figure 7. The Transition of the Spinal Radial Glial Progenitors from the Embryo-Specific Expansion to the Larva-Specific Commitment Phase Is Controlled by a Bidirectional Switch between miR-132 and Ctbp2

Schematic illustration of the proposed model. Curves are based on experimental expression data (Figures 1B and 6A).

See also Figures S5 and S6.

feedback loop involving Rest. At 48 hpf, the Gfap$^+$ glial progenitor pool and Notch signaling in these cells reach their developmental maximum. Significant molecular changes, however, take place in the Gfap$^+$ glial progenitors at this point: Ctbp2 rises significantly, and miR-132 expression becomes considerably higher and reaches a critical threshold to suppress Ctbp2 expression. This coincides with a drop in Rest levels (Gates et al., 2010). Together, these events might explain, at least partially, the interruption of the positive feedback regulation between Ctbp2 and miR-132 (Figure 7). The negative feed-forward regulation of miR-132 over Ctbp2 takes over, and the strongly increased miR-132 levels efficiently silence Ctbp2, eventually leading to the dampening of the Notch signaling and restriction of the Gfap$^+$ glial progenitors. In essence, the described pathway underlies a bimodal (increasing, then decreasing) Notch signaling switch in the Gfap$^+$ glial progenitor population (Figure 7). Notch bimodal signals are required for the unambiguous specification of progenitor/progeny pools (Bu et al., 2013; Chapouton et al., 2010). In the spinal cord, as shown here, this switch underlies another key cell fate choice: the dynamic transition of the radial glial progenitors toward a more restricted cell fate. It also coincides with the conversion of the primitive lumen into the mature central canal of the spinal cord (Kim et al., 2008b; Sevc et al., 2009). Postmitotic radial glial progenitors participate in these morphogenetic events as they lose their contacts with the ventricular zone, thus allowing the primitive lumen to descent ventrally and diminish in size to form the more confined central canal (Kondrychyn et al., 2013; Sevc et al., 2009). Thus, the miR-132-regulated signaling cascade ultimately contributes to this important developmental event (Hudish et al., 2013).

Up- or downregulation of key components of the circuit, i.e., Ctbp2, Sirt1, and Notch signaling itself, mimic the miR-132 loss- and gain-of-function phenotypes in the glial progenitors. *her4* expression and the balance of the Gfap$^+$/Olig2$^+$ cell populations corroborated the in vivo relevance of the molecular links between miR-132 and Notch signaling. Morpholino injections can lead to p53-related "off-target" phenotypes. However, nonspecific effects would not be able to explain with such consistency the bidirectional changes we observed regarding the key phenotypes we describe here (shifts in cell fate, glial arborization, *her4* expression). The use of multiple morpholinos against a single target, the rescues, and the target protector experiments confirm the specificity of our observations.

miRNAs are generally believed to simultaneously regulate multiple targets (Conaco et al., 2006). Apart from Ctbp2, other possible miR-132 targets are p250GAP (Vo et al., 2005; Wayman et al., 2008), MeCP2 (Klein et al., 2007), FOXP2 (Clovis et al., 2012), PTEN, FOXO3 (Wong et al., 2013), FOXO1A (Lau et al., 2013), and AchE (Shaked et al., 2009). Our data, however, provide convincing evidence that Ctbp2 is a core actor in the miR-132-dependent cascade regulating Notch-mediated signaling in the radial glial cells. The most direct proof comes from the target protection experiments, where blocking the miR-132 binding sites in the 3′ UTR of *ctbp2* completely mimics the phenotypes observed on both Ctbp2 gain of function and miR-132 loss of function.

Ctbp2 is a highly conserved transcriptional regulator (the zebrafish Ctbp2 protein shares more than 90% amino acid identity with its mammalian orthologs) (Van Hateren et al., 2006). Ctbp2 mainly acts as transcriptional corepressor through recruitment of histone deacetylases (Chinnadurai, 2002). It is interesting that CTBP2 is highly expressed in proliferating neural progenitors lining the lumen of the spinal cord during avian and mammalian development, while CTBP2 knockout mice fail to complete the closure of the neural tube and die at E10.5 (Hildebrand and Soriano, 2002; Van Hateren et al., 2006). Accordingly, we found that Sirt1 genetically interacts with miR-132 and Ctbp2 in Notch regulation and maintenance of the Gfap$^+$/Olig2$^+$ balance. SIRT1 has been shown to dampen Notch signaling by deacetylating

(I) Effect on Ctbp2 and miR-132 expression on UV illumination of the photomorpholino-injected groups at 34 and 56 hpf. All samples were analyzed at 60 hpf. Values were compared to the non-UV-treated group.

In (B), (D), and (F), values were normalized to the geometric mean of *ef1a*, *b2m*, and *actin* (for *ctbp2*); and in (C), (D), (E), and (I), values were normalized to the U6 small nuclear RNA expression (for miR-132) and expressed as fold change compared to the control group. All values are presented as mean ± SEM. *$p < 0.05$; **$p < 0.01$; ***$p < 0.001$; ns, nonsignificant. See also Figure S5.

the Notch intracellular domain, leading to its proteasomal degradation (Guarani et al., 2011), and also by repressing Notch target gene transcription via heterochromatin formation together with the histone demethylase LSD1 (Mulligan et al., 2011).

While our data provide a good mechanistic explanation for the strong downregulation of Ctbp2 after 48 hpf and for the physiological relevance of miR-132 in this process, the question of which molecular factors drive the significant posttranscriptional upregulation of Ctbp2 from 24 to 48 hpf remains unanswered, but posttranslational regulation and proteasomal degradation (Liang et al., 2011; Wei et al., 2011) are factors to be considered.

Another aspect that deserves further study is the role of miR-132 loss of function beyond the maintenance of Gfap$^+$ glia as multipotent progenitors and the restriction of oligodendrocyte precursors studied here. Previous research has shown that radial glial maturation, as assessed by the Gfap$^+$/Olig2$^+$ ratio (Kim et al., 2008b), radial glial arborization, process elongation, and myelin gene expression (including Mbp), evolves in synchrony with the progression of their cell cycle or differentiation (Kim et al., 2008a; Kosodo and Huttner, 2009). It is, therefore, not unreasonable to suggest that aspects of the different miR-132 loss-of-function phenotypes that we report here may be causally related to the deficits associated with radial glial maturation, but further work is certainly required in order to evaluate to what extent this claim holds true for all aspects of the phenotypes.

In conclusion, our work identifies a regulatory pathway involving miR-132 and the miR-132 target Ctbp2, as well as Rest and Sirt1, which explains the dynamics of Notch signaling to set the timing of early radial glial differentiation and maturation in the developing spinal cord. miR-132 downregulation has also been associated with several CNS disorders, including Alzheimer's disease (AD), multiple sclerosis (MS), and ischemic stroke, paralleling increased CTBP2 and Notch levels (Desai et al., 2009; John et al., 2002; Lau et al., 2013; Lescher et al., 2012; Lusardi et al., 2010; Nagarsheth et al., 2006; Tseveleki et al., 2010; Wang et al., 2009). These disorders are characterized by compromised neuronal regeneration, impaired myelination, and neurodegeneration; and it is interesting that activation of SIRT1 has been proposed as a therapeutic approach in AD, MS, Parkinson's disease, and stroke (Bonda et al., 2011; Donmez, 2012; Nimmagadda et al., 2013). Thus, while the regulation of Notch signaling by miR-132 is clearly essential in early spinal cord development, existing evidence in the literature suggests that this pathway may also turn out to be part of a general response to neurodegenerative alterations in the CNS, providing an example of how understanding developmentally relevant pathways might also be helpful to delineate mechanisms of disease in the adulthood.

EXPERIMENTAL PROCEDURES

Ethical Approval

All animal protocols were approved by the Ethical Committee of the University of Leuven (KU Leuven, Leuven, Belgium).

Glial Arborization Phenotypic Scoring

Gfap$^+$ glial processes within the region between somites 10 and 15 (S10–S15) were monitored for any deviation from the wild-type arborization structure, as this region was the most representative one concerning aberrant glial branching. Larvae would be scored as having glial arborization defects if one or more defective processes were observed.

DAPT Treatment

For Notch inhibition, 24-hpf-old embryos were incubated in medium containing DAPT (Merck Millipore International; 5 μg/ml if not otherwise specified) or vehicle control (DMSO, 0.05% if not otherwise stated) at 28.5°C until the stage of analysis.

In Silico Predictions

miR-132 candidate targets were first predicted using miRNA Viewer (release April 2005, zebrafish genome-adapted miRanda [John et al., 2004]) and Targetspy (Release 1.0 October 2009 [Sturm et al., 2010]) and then the 3′ UTRs of the orthologous genes in zebrafish, mouse, or human were obtained from the National Center for Biotechnology Information and searched for putative miR-132 MREs (Bartel, 2009). Relevance to Notch signaling pathway was assessed through literature mining.

Photomorpholino and Light Exposure

The sense photo-morpholino (5′- TCATGGCTTTGPTTGACAAACAC -3′) was purchased from Gene Tools LLC. Prior to use, the stock solution was heated for 30 min at 65°C. For duplexation, the photo-morpholino was mixed with the antisense CTBP2 ATG morpholino at a 1.1:1.0 ratio, vortexed, incubated for 10 min at room temperature, and diluted in water to a final concentration of 0.8 mM. For UV exposure, a HBO light source was used. In short, the HBO lamp housing of an Axioplan2 fluorescence microscope was outfitted with an Ushio 103/2 gas discharge lamp. For selecting UV light, a bandpass filter (325–375 nm) was used. At the indicated time point, fish were placed in the parallel part of the light path using an empty position at a distance of 7 cm from the objective revolver and irradiated for 8 min. Samples were analyzed at 60 hpf.

FACS

For the FACS sorting experiments, approximately 300–500 larvae were trypsinized in 0.25% Trypsin for 60 min at 28°C; diluted in 10 ml PBS; filtered over a 40 μm nylon mesh; centrifuged for 7 min at 1,300 rpm; and resuspended in 1 ml PBS supplemented with 1% BSA. The sorting was performed using FACS ARIA III (BD Biosciences). We collected 100,000 GFP$^+$ cells per sample in 1 ml Trizol.

Touch Escape Response

Touch escape response was assessed in newly hatched larvae at 52 hpf. Larvae were kept in separate gridded Petri dishes (1 cm spaced cross-grid lines). Escape response was elicited by tactile stimulation on the trunk with a hand-held poker. Responsiveness was measured as the swimming distance away from the stimulus. Behavior was scored as impaired when the distance was less than or equal to the half of the average distance swam by the control fish.

Image Acquisition

Bright-field images were acquired using a Leica DM2500 M light microscope. Confocal images were acquired using a Nikon A1R Eclipse Ti confocal microscope.

Statistical Analyses

When two nominal variables were analyzed, the chi-square test of independence was used (e.g., individuals with defects/individuals with no defects, red fluorescent cells/green fluorescent cells, and normal/impaired escape response). In the case of analyzing two measurable variables, the Student's t test was used (e.g., luciferase assays, overexpression/knockdown semi-quantitative PCR analysis). For comparisons between means of multiple measurable variables, the one-way ANOVA for multiple testing with Tukey's multiple comparison post hoc test was used (e.g., myelinated fiber length ratios, endogenous expression analyses, cell numbers, lumen and canal diameter); and when two interfering factors were considered in the analysis, the two-way ANOVA with Bonferroni's post hoc correction was used (DAPT dose-response in miR-132 morphants, Gfap$^+$/Olig2$^+$ cell numbers in DAPT-treated miR-132 morphants and controls). All data are representative of at least three independent experiments.

SUPPLEMENTAL INFORMATION

Supplemental Information includes Supplemental Experimental Procedures and six figures and can be found with this article online at http://dx.doi.org/10.1016/j.devcel.2014.07.006.

ACKNOWLEDGMENTS

We thank Drs. A. Zwijsen, P. Verstreken, B. Hassan, and A. Sierksma for critical feedback. The research was supported by the European Research Council, the Queen Elisabeth Foundation, the Fonds voor Wetenschappelijk Onderzoek, KU Leuven and VIB, and a Methusalem grant from KU Leuven and the Flemish Government (to B.D.S.). B.D.S. is supported by the Bax-Vanluffelen Chair for Alzheimer Disease. We thank Drs. B. Appel, P. Raymond, U. Strähle, E. Yaksi, R. Collins, H. Gerhardt, and C. Buckley for fish lines and reagents. The monoclonal antibody against Isl1, developed by T.M. Jessell and S. Brenner-Morton, was obtained from the Developmental Studies Hybridoma Bank, (created by the *Eunice Kennedy Shriver* National Institute of Child Health and Human Development and maintained at the University of Iowa, Department of Biology, Iowa City, IA 52242). J. Vandenbempt, F. Hendrickx, and K. Lambaerts provided expert fish care. S. Munck assisted with the photomorpholino experiments. Confocal microscopy equipment was acquired through a Hercules Type 1 AKUL/09/037 to W. Annaert.

Received: July 1, 2013
Revised: June 25, 2014
Accepted: July 10, 2014
Published: August 14, 2014

REFERENCES

Barresi, M.J., Burton, S., Dipietrantonio, K., Amsterdam, A., Hopkins, N., and Karlstrom, R.O. (2010). Essential genes for astroglial development and axon pathfinding during zebrafish embryogenesis. Dev. Dyn. *239*, 2603–2618.

Barry, D.S., Pakan, J.M., O'Keeffe, G.W., and McDermott, K.W. (2013). The spatial and temporal arrangement of the radial glial scaffold suggests a role in axon tract formation in the developing spinal cord. J. Anat. *222*, 203–213.

Bartel, D.P. (2009). MicroRNAs: target recognition and regulatory functions. Cell *136*, 215–233.

Bonda, D.J., Lee, H.G., Camins, A., Pallàs, M., Casadesus, G., Smith, M.A., and Zhu, X. (2011). The sirtuin pathway in ageing and Alzheimer disease: mechanistic and therapeutic considerations. Lancet Neurol. *10*, 275–279.

Bu, P., Chen, K.Y., Chen, J.H., Wang, L., Walters, J., Shin, Y.J., Goerger, J.P., Sun, J., Witherspoon, M., Rakhilin, N., et al. (2013). A microRNA miR-34a-regulated bimodal switch targets Notch in colon cancer stem cells. Cell Stem Cell *12*, 602–615.

Buckley, C.E., Marguerie, A., Alderton, W.K., and Franklin, R.J. (2010). Temporal dynamics of myelination in the zebrafish spinal cord. Glia *58*, 802–812.

Campbell, K., and Götz, M. (2002). Radial glia: multi-purpose cells for vertebrate brain development. Trends Neurosci. *25*, 235–238.

Chapouton, P., Skupien, P., Hesl, B., Coolen, M., Moore, J.C., Madelaine, R., Kremmer, E., Faus-Kessler, T., Blader, P., Lawson, N.D., and Bally-Cuif, L. (2010). Notch activity levels control the balance between quiescence and recruitment of adult neural stem cells. J. Neurosci. *30*, 7961–7974.

Chinnadurai, G. (2002). CtBP, an unconventional transcriptional corepressor in development and oncogenesis. Mol. Cell *9*, 213–224.

Clovis, Y.M., Enard, W., Marinaro, F., Huttner, W.B., and De Pietri Tonelli, D. (2012). Convergent repression of Foxp2 3'UTR by miR-9 and miR-132 in embryonic mouse neocortex: implications for radial migration of neurons. Development *139*, 3332–3342.

Conaco, C., Otto, S., Han, J.J., and Mandel, G. (2006). Reciprocal actions of REST and a microRNA promote neuronal identity. Proc. Natl. Acad. Sci. USA *103*, 2422–2427.

Desai, M.K., Sudol, K.L., Janelsins, M.C., Mastrangelo, M.A., Frazer, M.E., and Bowers, W.J. (2009). Triple-transgenic Alzheimer's disease mice exhibit region-specific abnormalities in brain myelination patterns prior to appearance of amyloid and tau pathology. Glia *57*, 54–65.

Donmez, G. (2012). The neurobiology of sirtuins and their role in neurodegeneration. Trends Pharmacol. Sci. *33*, 494–501.

Gates, K.P., Mentzer, L., Karlstrom, R.O., and Sirotkin, H.I. (2010). The transcriptional repressor REST/NRSF modulates hedgehog signaling. Dev. Biol. *340*, 293–305.

Geling, A., Steiner, H., Willem, M., Bally-Cuif, L., and Haass, C. (2002). A gamma-secretase inhibitor blocks Notch signaling in vivo and causes a severe neurogenic phenotype in zebrafish. EMBO Rep. *3*, 688–694.

Givogri, M.I., de Planell, M., Galbiati, F., Superchi, D., Gritti, A., Vescovi, A., de Vellis, J., and Bongarzone, E.R. (2006). Notch signaling in astrocytes and neuroblasts of the adult subventricular zone in health and after cortical injury. Dev. Neurosci. *28*, 81–91.

Guarani, V., Deflorian, G., Franco, C.A., Krüger, M., Phng, L.K., Bentley, K., Toussaint, L., Dequiedt, F., Mostoslavsky, R., Schmidt, M.H., et al. (2011). Acetylation-dependent regulation of endothelial Notch signalling by the SIRT1 deacetylase. Nature *473*, 234–238.

Hildebrand, J.D., and Soriano, P. (2002). Overlapping and unique roles for C-terminal binding protein 1 (CtBP1) and CtBP2 during mouse development. Mol. Cell. Biol. *22*, 5296–5307.

Hudish, L.I., Blasky, A.J., and Appel, B. (2013). miR-219 regulates neural precursor differentiation by direct inhibition of apical par polarity proteins. Dev. Cell *27*, 387–398.

Jimenez-Mateos, E.M., Bray, I., Sanz-Rodriguez, A., Engel, T., McKiernan, R.C., Mouri, G., Tanaka, K., Sano, T., Saugstad, J.A., Simon, R.P., et al. (2011). miRNA Expression profile after status epilepticus and hippocampal neuroprotection by targeting miR-132. Am. J. Pathol. *179*, 2519–2532.

John, G.R., Shankar, S.L., Shafit-Zagardo, B., Massimi, A., Lee, S.C., Raine, C.S., and Brosnan, C.F. (2002). Multiple sclerosis: re-expression of a developmental pathway that restricts oligodendrocyte maturation. Nat. Med. *8*, 1115–1121.

John, B., Enright, A.J., Aravin, A., Tuschl, T., Sander, C., and Marks, D.S. (2004). Human microRNA targets. PLoS Biol. *2*, e363.

Johnson, R., and Buckley, N.J. (2009). Gene dysregulation in Huntington's disease: REST, microRNAs and beyond. Neuromolecular Med. *11*, 183–199.

Kawase-Koga, Y., Otaegi, G., and Sun, T. (2009). Different timings of Dicer deletion affect neurogenesis and gliogenesis in the developing mouse central nervous system. Dev. Dyn. *238*, 2800–2812.

Kim, H., Kim, S., Chung, A.Y., Bae, Y.K., Hibi, M., Lim, C.S., and Park, H.C. (2008a). Notch-regulated perineurium development from zebrafish spinal cord. Neurosci. Lett. *448*, 240–244.

Kim, H., Shin, J., Kim, S., Poling, J., Park, H.C., and Appel, B. (2008b). Notch-regulated oligodendrocyte specification from radial glia in the spinal cord of zebrafish embryos. Dev. Dyn. *237*, 2081–2089.

Kim, A.H., Reimers, M., Maher, B., Williamson, V., McMichael, O., McClay, J.L., van den Oord, E.J., Riley, B.P., Kendler, K.S., and Vladimirov, V.I. (2010). MicroRNA expression profiling in the prefrontal cortex of individuals affected with schizophrenia and bipolar disorders. Schizophr. Res. *124*, 183–191.

Klein, M.E., Lioy, D.T., Ma, L., Impey, S., Mandel, G., and Goodman, R.H. (2007). Homeostatic regulation of MeCP2 expression by a CREB-induced microRNA. Nat. Neurosci. *10*, 1513–1514.

Kondrychyn, I., Teh, C., Sin, M., and Korzh, V. (2013). Stretching morphogenesis of the roof plate and formation of the central canal. PLoS ONE *8*, e56219.

Kosodo, Y., and Huttner, W.B. (2009). Basal process and cell divisions of neural progenitors in the developing brain. Dev. Growth Differ. *51*, 251–261.

Lau, P., Bossers, K., Janky, R., Salta, E., Frigerio, C.S., Barbash, S., Rothman, R., Sierksma, A.S., Thathiah, A., Greenberg, D., et al. (2013). Alteration of the microRNA network during the progression of Alzheimer's disease. EMBO Mol. Med. *5*, 1613–1634.

Lee, S.T., Chu, K., Im, W.S., Yoon, H.J., Im, J.Y., Park, J.E., Park, K.H., Jung, K.H., Lee, S.K., Kim, M., and Roh, J.K. (2011). Altered microRNA regulation in Huntington's disease models. Exp. Neurol. *227*, 172–179.

Lescher, J., Paap, F., Schultz, V., Redenbach, L., Scheidt, U., Rosewich, H., Nessler, S., Fuchs, E., Gärtner, J., Brück, W., and Junker, A. (2012). MicroRNA regulation in experimental autoimmune encephalomyelitis in mice and marmosets resembles regulation in human multiple sclerosis lesions. J. Neuroimmunol. *246*, 27–33.

Liang, H., Fekete, D.M., and Andrisani, O.M. (2011). CtBP2 downregulation during neural crest specification induces expression of Mitf and REST, resulting in melanocyte differentiation and sympathoadrenal lineage suppression. Mol. Cell. Biol. *31*, 955–970.

Lusardi, T.A., Farr, C.D., Faulkner, C.L., Pignataro, G., Yang, T., Lan, J., Simon, R.P., and Saugstad, J.A. (2010). Ischemic preconditioning regulates expression of microRNAs and a predicted target, MeCP2, in mouse cortex. J. Cereb. Blood Flow Metab. *30*, 744–756.

Mulligan, P., Yang, F., Di Stefano, L., Ji, J.Y., Ouyang, J., Nishikawa, J.L., Toiber, D., Kulkarni, M., Wang, Q., Najafi-Shoushtari, S.H., et al. (2011). A SIRT1-LSD1 corepressor complex regulates Notch target gene expression and development. Mol. Cell *42*, 689–699.

Nagarsheth, M.H., Viehman, A., Lippa, S.M., and Lippa, C.F. (2006). Notch-1 immunoexpression is increased in Alzheimer's and Pick's disease. J. Neurol. Sci. *244*, 111–116.

Nimmagadda, V.K., Bever, C.T., Vattikunta, N.R., Talat, S., Ahmad, V., Nagalla, N.K., Trisler, D., Judge, S.I., Royal, W., 3rd, Chandrasekaran, K., et al. (2013). Overexpression of SIRT1 protein in neurons protects against experimental autoimmune encephalomyelitis through activation of multiple SIRT1 targets. J. Immunol. *190*, 4595–4607.

Park, H.C., Mehta, A., Richardson, J.S., and Appel, B. (2002). olig2 is required for zebrafish primary motor neuron and oligodendrocyte development. Dev. Biol. *248*, 356–368.

Park, H.C., Shin, J., Roberts, R.K., and Appel, B. (2007). An olig2 reporter gene marks oligodendrocyte precursors in the postembryonic spinal cord of zebrafish. Dev. Dyn. *236*, 3402–3407.

Peng, C., Li, N., Ng, Y.K., Zhang, J., Meier, F., Theis, F.J., Merkenschlager, M., Chen, W., Wurst, W., and Prakash, N. (2012). A unilateral negative feedback loop between miR-200 microRNAs and Sox2/E2F3 controls neural progenitor cell-cycle exit and differentiation. J. Neurosci. *32*, 13292–13308.

Petit, A., Sanders, A.D., Kennedy, T.E., Tetzlaff, W., Glattfelder, K.J., Dalley, R.A., Puchalski, R.B., Jones, A.R., and Roskams, A.J. (2011). Adult spinal cord radial glia display a unique progenitor phenotype. PLoS ONE *6*, e24538.

Pogoda, H.M., Sternheim, N., Lyons, D.A., Diamond, B., Hawkins, T.A., Woods, I.G., Bhatt, D.H., Franzini-Armstrong, C., Dominguez, C., Arana, N., et al. (2006). A genetic screen identifies genes essential for development of myelinated axons in zebrafish. Dev. Biol. *298*, 118–131.

Sevc, J., Daxnerová, Z., and Miklosová, M. (2009). Role of radial glia in transformation of the primitive lumen to the central canal in the developing rat spinal cord. Cell. Mol. Neurobiol. *29*, 927–936.

Shaked, I., Meerson, A., Wolf, Y., Avni, R., Greenberg, D., Gilboa-Geffen, A., and Soreq, H. (2009). MicroRNA-132 potentiates cholinergic anti-inflammatory signaling by targeting acetylcholinesterase. Immunity *31*, 965–973.

Shin, J., Park, H.C., Topczewska, J.M., Mawdsley, D.J., and Appel, B. (2003). Neural cell fate analysis in zebrafish using olig2 BAC transgenics. Methods Cell Sci. *25*, 7–14.

Staton, A.A., and Giraldez, A.J. (2011). Use of target protector morpholinos to analyze the physiological roles of specific miRNA-mRNA pairs in vivo. Nat. Protoc. *6*, 2035–2049.

Sturm, M., Hackenberg, M., Langenberger, D., and Frishman, D. (2010). TargetSpy: a supervised machine learning approach for microRNA target prediction. BMC Bioinformatics *11*, 292.

Takke, C., Dornseifer, P., v Weizsäcker, E., and Campos-Ortega, J.A. (1999). her4, a zebrafish homologue of the Drosophila neurogenic gene E(spl), is a target of NOTCH signalling. Development *126*, 1811–1821.

Tallafuss, A., Gibson, D., Morcos, P., Li, Y., Seredick, S., Eisen, J., and Washbourne, P. (2012). Turning gene function ON and OFF using sense and antisense photo-morpholinos in zebrafish. Development *139*, 1691–1699.

Taylor, M.K., Yeager, K., and Morrison, S.J. (2007). Physiological Notch signaling promotes gliogenesis in the developing peripheral and central nervous systems. Development *134*, 2435–2447.

Trevarrow, B., Marks, D.L., and Kimmel, C.B. (1990). Organization of hindbrain segments in the zebrafish embryo. Neuron *4*, 669–679.

Tseveleki, V., Rubio, R., Vamvakas, S.S., White, J., Taoufik, E., Petit, E., Quackenbush, J., and Probert, L. (2010). Comparative gene expression analysis in mouse models for multiple sclerosis, Alzheimer's disease and stroke for identifying commonly regulated and disease-specific gene changes. Genomics *96*, 82–91.

Van Hateren, N., Shenton, T., and Borycki, A.G. (2006). Expression of avian C-terminal binding proteins (Ctbp1 and Ctbp2) during embryonic development. Dev. Dyn. *235*, 490–495.

Vo, N., Klein, M.E., Varlamova, O., Keller, D.M., Yamamoto, T., Goodman, R.H., and Impey, S. (2005). A cAMP-response element binding protein-induced microRNA regulates neuronal morphogenesis. Proc. Natl. Acad. Sci. USA *102*, 16426–16431.

Wanet, A., Tacheny, A., Arnould, T., and Renard, P. (2012). miR-212/132 expression and functions: within and beyond the neuronal compartment. Nucleic Acids Res. *40*, 4742–4753.

Wang, S., Sdrulla, A.D., diSibio, G., Bush, G., Nofziger, D., Hicks, C., Weinmaster, G., and Barres, B.A. (1998). Notch receptor activation inhibits oligodendrocyte differentiation. Neuron *21*, 63–75.

Wang, L., Chopp, M., Zhang, R.L., Zhang, L., Letourneau, Y., Feng, Y.F., Jiang, A., Morris, D.C., and Zhang, Z.G. (2009). The Notch pathway mediates expansion of a progenitor pool and neuronal differentiation in adult neural progenitor cells after stroke. Neuroscience *158*, 1356–1363.

Wayman, G.A., Davare, M., Ando, H., Fortin, D., Varlamova, O., Cheng, H.Y., Marks, D., Obrietan, K., Soderling, T.R., Goodman, R.H., and Impey, S. (2008). An activity-regulated microRNA controls dendritic plasticity by down-regulating p250GAP. Proc. Natl. Acad. Sci. USA *105*, 9093–9098.

Wei, Z., Chigurupati, S., Arumugam, T.V., Jo, D.G., Li, H., and Chan, S.L. (2011). Notch activation enhances the microglia-mediated inflammatory response associated with focal cerebral ischemia. Stroke *42*, 2589–2594.

Wong, H.K., Veremeyko, T., Patel, N., Lemere, C.A., Walsh, D.M., Esau, C., Vanderburg, C., and Krichevsky, A.M. (2013). De-repression of FOXO3a death axis by microRNA-132 and -212 causes neuronal apoptosis in Alzheimer's disease. Hum. Mol. Genet. *22*, 3077–3092.

Wu, J., and Xie, X. (2006). Comparative sequence analysis reveals an intricate network among REST, CREB and miRNA in mediating neuronal gene expression. Genome Biol. *7*, R85.

Yeo, S.Y., Kim, M., Kim, H.S., Huh, T.L., and Chitnis, A.B. (2007). Fluorescent protein expression driven by her4 regulatory elements reveals the spatiotemporal pattern of Notch signaling in the nervous system of zebrafish embryos. Dev. Biol. *301*, 555–567.

Zannino, D.A., and Appel, B. (2009). Olig2+ precursors produce abducens motor neurons and oligodendrocytes in the zebrafish hindbrain. J. Neurosci. *29*, 2322–2333.

Zhang, Q., Wang, S.Y., Fleuriel, C., Leprince, D., Rocheleau, J.V., Piston, D.W., and Goodman, R.H. (2007). Metabolic regulation of SIRT1 transcription via a HIC1:CtBP corepressor complex. Proc. Natl. Acad. Sci. USA *104*, 829–833.